Assessment of the colored dissolved organic matter in coastal waters from ocean color remote sensing

Hubert Loisel, Vincent Vantrepotte, David Dessailly, Xavier Meriaux

Assessment of the colored dissolved organic matter in coastal waters from ocean color remote sensing

Hubert Loisel,[1,2,3,*] Vincent Vantrepotte,[3] David Dessailly,[3] and Xavier Mériaux[3]

[1]*Institut de Recherche pour le Développement (IRD), Université de Toulouse, UPS (OMP), UMR 5566 LEGOS, 14 av. Edouard Belin, 31400 Toulouse, France*

[2]*Space Technology Institute (STI), Vietnam Academy of Science & Technology (VAST), 18 Hoang Quoc Viet, Cau Giay, Ha Noi, Vietnam*

[3]*Université. Lille Nord de France, ULCO, LOG, CNRS – UMR8187, F-62930 Wimereux, France*

[*]*hubert.loisel@univ-littoral.fr*

Abstract: Knowledge on absorption by colored dissolved organic matter, a_{cdom}, spatio-temporal variability in coastal areas is of fundamental importance in many field of researches related to biogeochemical cycles studies, coastal areas management, as well as land and water interactions in the coastal domain. A new method, based on the theoretical link between the vertical attenuation coefficient, K_d, and the absorption coefficient, has been developed to assess a_{cdom}. This method, confirmed from radiative transfer simulations and in situ measurements, and tested on an independent *in situ* data set (N = 126), allows a_{cdom} to be assessed with a Mean Relative Absolute Difference, MRAD, of 33% over two order of magnitude (from 0.01 to 1.16 m^{-1}). In the frame of ocean color observation, K_d is not directly measured but estimated from the remote sensing reflectance, R_{rs}. Based on 109 satellite (SeaWiFS) and *in situ* coincident (i.e. match-up) data points a_{cdom} is retrieved with a MRAD value of 37%. This simple model generally presents slightly better performances than recently developed empirical or semi-analytical algorithms.

OCIS codes: (010.4450) Oceanic optics; (010.1690) Color; (010.1030) Absorption.

References and links

1. J. T. O. Kirk, *Light and Photosynthesis in aquatic ecosystems* (Academic, 1994).
2. N. V. Blough and R. Del Vecchio, "Chromophoric DOM in the coastal environment," in *Biogeochemistry of Marine Dissolved Organic Matter*, D. A. Hansell and C. A. Carslon, ed. (Academic, 2002).
3. V. Vantrepotte, C. Brunet, X. Mériaux, E. Lécuyer, V. Vellucci, and R. Santer, "Bio-optical properties of coastal waters in the Eastern English Channel," Estuar. Coast. Shelf Sci. **72**(1–2), 201–212 (2007).
4. A. Mannino, M. Russ, and S. Hooker, "Algorithm development and validation for satellite-derived distributions of DOC and CDOM in the US Middle Atlantic Bight," J. Geophys. Res. **113**(C7), C07051 (2008).
5. C. E. Del Castillo, "Remote Sensing of Colored Dissolved Organic Matter in Coastal Environments," in *Remote Sensing of Aquatic Coastal Environments*, R. M. Miller, C. E. Del Castillo, and B. McKee, ed. (Academic, 2004).
6. C. Fichot and R. Benner, "The spectral slope coefficient of chromophoric dissolved organic matter ($S_{275\text{-}295}$) as a tracer of terrigenous dissolved organic carbon in river-influenced ocean margins," Limnol. Oceanogr. **57**(5), 1453–1466 (2012).
7. K. L. Carder, S. K. Hawes, K. A. Baker, R. C. Smith, R. G. Steward, and B. G. Mitchell, "Reflectance model for quantifying chlorophyll-a in the presence of productivity degradation products," J. Geophys. Res. **96**(C11), 20599–20611 (1991).
8. D. A. Siegel, S. Maritorena, N. B. Nelson, M. J. Behrenfeld, and C. R. McClain, "Colored dissolved organic matter and its influence on the satellite-based characterization of the ocean biosphere," Geophys. Res. Lett. **32**(20), L20605 (2005), doi:10.1029/2005GL024310.
9. A. Morel and B. Gentili, "A simple band ratio technique to quantify the colored dissolved and detrital organic material from ocean color remotely sensed data," Remote Sens. Environ. **113**(5), 998–1011 (2009), doi:10.1016/j.rse.2009.01.008.

#208531 - $15.00 USD Received 18 Mar 2014; revised 9 May 2014; accepted 9 May 2014; published 22 May 2014

10. C. A. Brown, Y. Huot, P. J. Werdell, B. Gentili, and H. Claustre, "The origin and global distribution of second order variability in satellite ocean color and its potential applications to algorithm development," Remote Sens. Environ. **112**(12), 4186–4203 (2008), doi:10.1016/j.rse.2008.06.008.
11. L. Hubert, B. Lubac, D. Dessailly, L. Duforêt-Gaurier, and V. Vantrepotte, "Effect of inherent optical properties variability on the chlorophyll retrieval from ocean color remote sensing: an in situ approach," Opt. Express **18**(20), 20949–20959 (2010).
12. Z. P. Lee, K. L. Carder, and R. A. Arnone, "Deriving inherent optical properties from water color: A multiband quasi-analytical algorithm for optically deep waters," Appl. Opt. **41**(27), 5755–5772 (2002).
13. S. A. Garver and D. A. Siegel, "Inherent optical property inversion of ocean color spectra and its biogeochemical interpretation 1. Time series from the Sargasso Sea," J. Geophys. Res. **102**(C8), 18607–18625 (1997).
14. S. Maritorena, D. A. Siegel, and A. R. Peterson, "Optimization of a semianalytical ocean color model for global-scale applications," Appl. Opt. **41**(15), 2705–2714 (2002).
15. D. A. Siegel, S. Maritorena, N. B. Nelson, and D. A. Hansell, "Global distribution and dynamics of colored dissolved and detrital organic materials," J. Geophys. Res. **107**(C12), 3228 (2002).
16. M. Babin, D. Stramski, G. M. Ferrari, H. Claustre, A. Bricaud, G. Obolensky, and N. Hoepffner, "Variations in the light absorption coefficients of phytoplankton, non-algal particles, and dissolved organic matter in coastal waters around Europe," J. Geophys. Res. **108**(C7), 3211 (2003), doi:10.1029/2001JC000882.
17. E. J. D'Sa, R. L. Miller, and C. Del Castillo, "Bio-optical properties and ocean color algorithms for coastal waters influenced by the Mississippi River during a cold front," Appl. Opt. **45**(28), 7410–7428 (2006).
18. E. Siswanto, J. Tang, H. Yamaguchi, Y.-H. Ahn, J. Ishizaka, S. Yoo, S.-W. Kim, Y. Kiyomoto, K. Yamada, C. Chiang, and H. Kawamura, "Empirical ocean-color algorithms to retrieve chlorophyll- a, total suspended matter, and colored dissolved organic matter absorption coefficient in the Yellow and East China Seas," J. Oceanogr. **67**(5), 627–650 (2011).
19. S. P. Tiwari and P. Shanmugam, "An optical model for the remote sensing of coloured dissolved organic matter in coastal/ocean waters," Estuar. Coast. Shelf Sci. **93**(4), 396–402 (2011).
20. S. Bélanger, M. Babin, and P. Larouche, "An empirical ocean color algorithm for estimating the contribution of chromophoric dissolved organic matter to total light absorption in optically complex waters," J. Geophys. Res. **113**(C4), C04027 (2008), doi:10.1029/2007JC004436.
21. H. Loisel and D. Stramski, "Estimation of the inherent optical properties of natural waters from the irradiance attenuation coefficient and reflectance in the presence of Raman scattering," Appl. Opt. **39**(18), 3001–3011 (2000).
22. Q. Dong, S. Shang, and Z. P. Lee, "An algorithm to retrieve absorption coefficient of chromophoric dissolved organic matter from ocean color," Remote Sens. Environ. **128**, 259–267 (2013).
23. A. Matsuoka, S. B. Hooker, A. Bricaud, B. Gentili, and M. Babin, "Estimating absorption coefficients of colored dissolved organic matter (CDOM) using a semi-analytical algorithm for southern Beaufort Sea waters: application to deriving concentrations of dissolved organic carbon from space," Biogeosciences **10**(2), 917–927 (2013).
24. IOCCG, "*Remote Sensing of Inherent Optical Properties: Fundamentals, Tests of Algorithms, and Applications*," in Reports of the International Ocean-Colour Coordinating Group, 5, Z. P. Lee, ed. IOCCG, Dartmouth, (2006).
25. P. J. Werdell and S. W. Bailey, "An improved in situ bio-optical data set for ocean color algorithm development and satellite data product validation," Remote Sens. Environ. **98**(1), 122–140 (2005).
26. B. Lubac, H. Loisel, N. Guiselin, R. Astoreca, L. F. Artigas, and X. Mériaux, "Hyperspectral and multispectral ocean color inversions to detect *Phaeocystis globosa* blooms in coastal waters," J. Geophys. Res. **113**, C06026 (2008), doi:10.1029/2007JC004451.
27. H. Loisel, X. Mériaux, A. Poteau, L. F. Artigas, B. Lubac, A. Gardel, J. Caillaud, and S. Lesourd, "Analyze of the inherent optical properties of French Guiana coastal waters for remote sensing applications," J. Coast. Res. **56**, 1532–1536 (2009).
28. V. Vantrepotte, H. Loisel, D. Dessailly, and X. Mériaux, "Optical classification of contrasted coastal waters," Remote Sens. Environ. **123**, 306–323 (2012), doi:10.1016/j.rse.2012.03.004.
29. J. T. O. Kirk, "Monte Carlo study of the nature of the under- water light field in, and the relationships between optical properties of, turbid yellow waters," Aust. J. Mar. Freshwater Res. **32**(4), 517–532 (1981).
30. J. T. O. Kirk, "Dependence of relationship between inherent and apparent optical properties of water on solar altitude," Limnol. Oceanogr. **29**(2), 350–356 (1984).
31. J. T. O. Kirk, "Volume scattering function, average cosines, and the underwater light field," Limnol. Oceanogr. **36**(3), 455–467 (1991).
32. H. R. Gordon, "Can the Lambert–Beer law be applied to the diffuse attenuation coefficient of ocean water," Limnol. Oceanogr. **34**(8), 1389–1409 (1989).
33. A. Morel and H. Loisel, "Apparent Optical properties of oceanic water: dependence on the molecular scattering contribution," Appl. Opt. **37**(21), 4765–4776 (1998).
34. H. R. Gordon and W. R. McCluney, "Estimation of the depth of sunlight penetration in the sea for remote sensing," Appl. Opt. **14**(2), 413–416 (1975).
35. S. Sathyendranath and T. Platt, "The spectral irradiance field at the surface and in the interior of the ocean: A model for applications in oceanography and remote sensing," J. Geophys. Res. **93**(C8), 9270–9280 (1988).

#208531 - $15.00 USD Received 18 Mar 2014; revised 9 May 2014; accepted 9 May 2014; published 22 May 2014

36. Z. P. Lee, K. Du, and R. Arnone, "A model for the diffuse attenuation coefficient of downwelling irradiance," J. Geophys. Res. **110**, C02016 (2005), doi:10.1029/2004JC002275.
37. A. Morel, "Optical modeling of the upper ocean in relation to its biogenous matter content (case 1 water)," J. Geophys. Res. **93**(C9), 10,749–10,768 (1988).
38. A. Morel and S. Maritorena, "Bio-optical properties of oceanic waters: A reappraisal," J. Geophys. Res. **106**(C4), 7163–7180 (2001).
39. A. Morel and L. Prieur, "Analysis of variations in ocean color," Limnol. Oceanogr. **22**(4), 709–722 (1977).
40. T. Zhang, F. Fell, Z. S. Liu, R. Preusker, J. Fischer, and M. X. He, "Evaluating the performance of artificial neural network techniques for pigment retrieval from ocean color in case I waters," J. Geophys. Res. **108**(C9), 3286 (2003), doi:10.1029/2002JC001638.
41. http://oceancolor.gsfc.nasa.gov/REPROCESSING/SeaWiFS/R5.1/k490_update.html.
42. C. Jamet, H. Loisel, and D. Dessailly, "Retrieval of the spectral diffuse attenuation coefficient Kd(λ) in open and coastal ocean waters using a neural network inversion," J. Geophys. Res. **117**(C10), C10023 (2012), doi:10.1029/2012JC008076.
43. K. S. Baker and R. C. Smith, "Bio-optical classification and model of natural waters. 2," Limnol. Oceanogr. **27**(3), 500–509 (1982).
44. M. S. Twardowski, E. Boss, J. M. Sullivan, and P. L. Donaghay, "Modeling the spectral shape of absorption by chromophoric dissolved organic matter," Mar. Chem. **89**(1-4), 69–88 (2004), doi:10.1016/j.marchem.2004.02.008.
45. D. Jolivet, D. Ramon, P.-Y. Deschamps, F. Steinmetz, B. Fougnie, and P. Henry, "How the ocean color products is limited by atmospheric correction," in Proceedings of Envisat Symposium 2007, Montreux, Switzerland (2007).
46. C. Hu, L. Feng, Z.-P. Lee, C. O. Davis, A. Mannino, C. R. McClain, and B. A. Franz, "Dynamic range and sensitivity requirements of satellite ocean color sensors: learning from the past," Appl. Opt. **51**(25), 6045–6062 (2012).
47. C. Jamet, H. Loisel, C. P. Kuchinke, K. Ruddick, G. Zibordi, and H. Feng, "Comparison of three SeaWiFS atmospheric correction algorithms for turbid waters using AERONET-OC measurements," Remote Sens. Environ. **115**(8), 1955–1965 (2011).
48. C. D. Mobley, *Light and Water: Radiative Transfer in Natural Waters* (Academic, 1994).
49. R. J. Hyndman and Y. Fan, "Sample Quantiles in Statistical Packages," Am. Stat. **50**(4), 361–365 (1996).
50. B. Lubac and H. Loisel, "Variability and classification of remote sensing reflectance spectra in the eastern English Channel and southern North Sea," Remote Sens. Environ. **110**(1), 45–58 (2007).
51. ESA-report, (ESA, 2012). http://earth.eo.esa.int/pcs/envisat/meris/documentation/meris_3rd_reproc/A879-NT-017ACR_v1.0.pdf.

1. Introduction

Colored dissolved organic matter (*CDOM*) (referred as yellow substances, Gelbstoff, or gilvin) refers to a complex mixture of water-soluble organic substances including mainly humic and fulvic acids. *CDOM* in coastal waters mainly originates from rivers and land washing, but can also be locally produced by phytoplankton as well as through the degradation processes of this marine organic matter [1–3]. *CDOM* plays a significant role for a variety of marine biogeochemical processes in coastal waters for instance through its controlling action of the marine light field available for phytoplankton primary production. *CDOM* is usually expressed as the absorption coefficient of a water sample filtered through a 0.2 µm filter, $a_{cdom}(\lambda)$ (in m^{-1}). The increasing exponential shape of *CDOM* absorption from long to short wavelengths induces that *CDOM* can prevent, when present in sufficient concentration, against photochemical damage induced by ultra violet radiations on aquatic organisms [see references in 2]. Previous works have also stressed that *CDOM,* especially in coastal water masses influenced by terrestrial inputs, can be used to assess the concentration of dissolved organic carbon, *DOC*, which represents the main reservoir of organic carbon in the ocean, still poorly quantified at global scale [4–6]. At last but not least, the presence of *CDOM* in waters has been shown to bias the estimation of the chlorophyll-a concentration, *Chla*, from ocean color remote sensing [7–11]. Loisel et al. [11] for instance illustrated that *Chla* is over-estimated in waters presenting higher *CDOM* concentrations than averaged values, and *vice versa*.

For the different reasons stated above, knowledge on the temporal and spatial distribution of *CDOM* is of great interest for marine sciences. Remote sensing of ocean color from space sensors is the dedicated tool for that purpose. However, due to their similar spectral shapes,

#208531 - $15.00 USD Received 18 Mar 2014; revised 9 May 2014; accepted 9 May 2014; published 22 May 2014

the non-algal particulate matter absorption, a_{nap}, and colored dissolved organic matter absorption, a_{cdom}, coefficients are difficult to distinguish from ocean color radiometric measurements. These two absorption coefficients are therefore usually gathered into one coefficient, the colored detrital matter absorption coefficient, a_{cdm}. Numerous efforts have been undertaken this last decade to assess a_{cdm} from remote sensing over open ocean and coastal waters, e.g, [9,12–14]. While, a_{cdm} can be assimilate to a_{cdom} over open ocean waters, in good approximation [15], this is not the case for coastal waters. In these optically complex aquatic environments, the contribution of a_{cdom} and a_{nap} to the total absorption (minus water) can drastically change at both regional and temporal scales [3,16]. This is due to the strong decoupling between source and sink processes controlling the variability of these two absorption coefficients. Considering the importance of *CDOM* in our understanding of biogeochemical processes occurring in coastal regions, recent algorithms have been developed to assess a_{cdom} from ocean color remote sensing over these optically complex waters. For instance, some empirical relationships have been established between a_{cdom} at different wavelengths and remote sensing reflectance, R_{rs}, ratios from data collected in various coastal environments [4,17–19]. Two steps algorithms, requiring the assessment of other inherent optical properties (IOPs) as intermediate products, have been also proposed. For instance, the $a_{cdom}(412)$ to the total absorption coefficient ratio, which has been parameterized as a function of R_{rs} at different wavelengths [20], could be used once the total absorption is assessed using another algorithm [12,21]. Others methods, aim at removing the contribution of particulate matter from $a_{cdm}(\lambda)$ based on estimates of the backscattering coefficient derived from dedicated algorithms [22,23].

The present paper aims at developing a new algorithm for assessing the absorption coefficient of colored dissolved organic matter at 412 nm, $a_{cdom}(412)$, from the diffuse attenuation coefficient, K_d, in coastal surface waters. The latter parameter can be estimated from *in situ* measurements of vertical profiles of downwelling irradiance, as well as from the inversion of ocean color remote sensing measurements. A synthetic data set, based on numerical radiative transfer simulations, as well as an *in situ* data set gathering measurements performed in contrasted coastal waters, are used for the theoretical development of the model. The performances of this new algorithm are evaluated using an independent *in situ* data set, and comparisons with other empirical and semi-analytical algorithms are provided.

2. Synthetic and in situ data set

Three different data sets are used for the present study. The first one (thereafter referred as DS1) is only used to develop the theoretical background of the algorithm. This synthetic data set has been generated from numerical simulations of the radiative transfer performed for various inherent optical properties (IOPs) and three different sun zenith angles (0°, 30°, and 60°). More details on this data set are provided in the IOCCG report 5 [24]. The second data set (DS2) only gathers *in situ* data collected in various and mainly coastal environments. For DS2 we use the NOMAD data set [25] together with data collected during other oceanographic cruises occurring in European and French Guiana coastal waters [16,26–28]. DS2 is divided into two sub-data sets, one for the algorithm development (DS2-D), the other for validation exercises (DS2-V). DS2-D and DS2-V encompass 80% (N = 505) and 20% (N = 126) of the data points and presents the same distribution in terms of $a_{cdom}(410)$ values. The last data set (DS3) used in the present study is the NOMAD SeaWiFS match-up data set (N = 109) which is composed by in situ $a_{cdom}(410)$ measurements and nearly simultaneous SeaWiFS derived remote sensing reflectance, R_{rs}, after atmospheric correction of the top of atmosphere signal.

#208531 - $15.00 USD Received 18 Mar 2014; revised 9 May 2014; accepted 9 May 2014; published 22 May 2014

Table 1. Mean, standard deviation, and range values of $a_{cdom}(410)$, $a_{cdom}(410)/a_{tot}(410)$, $K_d(410)$, $K_d(555)$, and $K_d(670)$ for the four considered data set (DS1 is the synthetic data set, DS2-D and DS2-V only gather *in situ* data, DS3 is the match-up data set which is composed by in situ $a_{cdom}(410)$ measurements and SeaWiFS retrieved R_{rs} parameters). N represents the number of data points. For in situ data (DS2-D and DS2-V) the blue wavelength is 412 nm.

	DS1	DS2-D	DS2-V	DS3
$a_{cdom}(410)$	0.51 ± 0.74	0.23 ± 0.26	0.24 ± 0.27	0.13 ± 0.20
	(N=500)	(N=505)	(N=126)	(N=109)
	[0.004;3.65]	[0.01;1.92]	[0.01;1.69]	[0.01;0.98]
$a_{cdom}(410)/a_{tot}(410)$	0.60 ± 0.18	0.53 ± 0.15	0.52 ± 0.15	
	(N=500)	(N=390)	(N=105)	
	[0.16;0.90]	[0.16;0.93]	[0.16;0.91]	
$K_d(410)$	0.83 ± 1.07	0.65 ± 0.87	0.72 ± 0.84	0.63 ± 0.74
	(N=500)	(N=505)	(N=126)	(N=109)
	[0.023;5.26]	[0.019; 5.23]	[0.011;3.83]	[0.029;2.095]
$K_d(555)$	0.23 ± 0.21	0.27 ± 0.32	0.30 ± 0.29	0.15 ± 0.16
	(N=500)	(N=505)	(N=126)	(N=109)
	[0.07;1.21]	[0.006;2.35]	[0.057;1.23]	[0.05;0.66]
$K_d(670)$	0.62 ± 0.17	0.85 ± 0.39	0.85 ± 0.29	
	(N=500)	(N=256)	(N=68)	
	[0.49;1.19]	[0.20;2.67]	[0.26;1.56]	

The mean, standard deviation, and range values of $K_d(\lambda)$, $a_{cdom}(410)$, and $a_{cdom}/a_{tot}(410)$, where a_{tot} is the sum of the particulate (a_p) and colored dissolved organic matter absorption (a_{cdom}) coefficients, for the different data sets are provided in Table 1. The $a_{cdom}(410)$ values cover a great range of variability, about three order of magnitude, for both the synthetic and i*n situ* data sets (Table 1). The mean and standard deviations values of $a_{cdom}(410)$ for DS1, DS2-D, DS2-V, and DS3 are 0.51 ± 0.74, 0.23 ± 0.26, 0.24 ± 0.27, and 0.13 ± 0.20 m^{-1}, respectively. The $a_{cdom}(410)$ values are equally distributed in DS2-D and DS2-V (with however some slight differences in the maximum values). The contribution of $a_{cdom}(410)$ to the total absorption process, represented by the a_{cdom}/a_{tot} ratio, are very similar among the three data sets and range between about 16 to 93% (Table 1). Besides the $a_{cdom}(410)$, $a_{tot}(410)$, $K_d(410)$, and $K_d(670)$ parameters gathered in the three considered data sets, DS2-V and DS3 also include the remote sensing reflectance, $R_{rs}(\lambda)$, values at the standard ocean color visible wavelengths (412, 443, 490, 510, 550, and 670 nm). $R_{rs}(\lambda)$ is considered for DS2-V and DS3 for validation purposes in the context of remote sensing applications, where R_{rs} is the input parameter used for calculating $K_d(\lambda)$ which represent the input parameter for deriving $a_{cdom}(410)$ from the present algorithm.

3. Theoretical background

The diffuse attenuation coefficient $K_d(\lambda)$ at a given wavelength, λ, is a function of inherent optical properties (IOPs) and illumination conditions at the sea surface [29–33]. Different parameterizations, based on extensive radiative transfer calculations, have been developed between K_d, IOPs, and the sun zenith angle, θ_0, at some specific depths, and for the first attenuation layer, which corresponds to the ocean surface layer that can be detected from an ocean color satellite sensor [34]. For example, simple parameterizations were proposed between K_d/a and b/a accounting for the sun zenith angles, where a and b are the total (including pure water coefficients) absorption and scattering coefficients, respectively [29,30]. Further parameterizations, were then aimed at including the effect of the variation of the total phase function (through the respective proportion between molecular and total scattering) as well as that of the aerosol optical thickness [31,33]. Based on the fact that the absorption and backscattering, b_b, coefficients can be estimated from space [24], K_d has also been parameterized as a function of a, b_b, and θ_0 [32,35,36]. Empirical parameterizations

#208531 - $15.00 USD Received 18 Mar 2014; revised 9 May 2014; accepted 9 May 2014; published 22 May 2014

between $K_d(\lambda)$ and the surface chlorophyll-a concentration, *Chla*, were also proposed [37,38] for Case 1 waters for which IOPs only depend on phytoplankton organisms and their associated material [39]. In this latter parameterization $K_d(\lambda)$ is decomposed as follows:

$$K_d(\lambda) = K_w(\lambda) + K_{d-bio}(\lambda) \quad (1)$$

where $K_w(\lambda)$ is the diffuse attenuation coefficient for a pure sea water body, and $K_{d\text{-}bio}(\lambda)$ is the contribution of all biogenic components (phytoplankton, heterotrophic bacteria, detritus, etc) and is modeled as a function of *Chla*.

Two main considerations drive the development of the present model to assess $a_{cdom}(412)$ from ocean color remote sensing observations. The first one relies on the fact that the diffuse attenuation coefficient, $K_d(\lambda)$, can now be estimated with a relatively good accuracy from the remote sensing reflectance, $R_{rs}(\lambda)$ [36,40–42]. For instance, based on an extensive *in situ* and synthetic data set, the average absolute relative error (i.e. uncertainty) value on the K_d assessment at 490 nm using 5 different approaches ranges between 14 and 32% [42]. The second motivation of the current approach is to take advantage of the fact that, for a given sun angle, $K_d(\lambda)$ can roughly be considered as a inherent optical properties in the surface layer, and then can be decomposed into different subcomponents [32,37,38,43]. Based on radiative transfer simulations Gordon [32] confirmed that by removing the dependence of $K_d(\lambda)$ on the structure of the incident light field at the sea surface, $K_d(\lambda)$ verifies the Lambert-Beer law near the sea surface.

4. Algorithm development

4.1 General formulation of the model

The different works referred previously emphasize that $K_d(\lambda)$ is mainly driven by the absorption coefficient, at first order. However, as soon as the $b/a(\lambda)$ (or $b_b/a(\lambda)$) ratio increases significantly, the attenuation of light through scattering processes cannot be neglected. Due to the exponential increase of $a_{cdom}(\lambda)$ from longer to shorter wavelengths, the present model will estimate $a_{cdom}(\lambda)$ at 412 nm. Based on these different considerations $K_d(412)$ can be expressed as follows:

$$K_d(412) = K_w(412) + f(a_{cdom}(412)) + \Delta_p(412) \quad (2)$$

where $K_w(412)$ is the diffuse attenuation coefficient for a pure sea water body, $f(a_{cdom}(412))$ is a function that only depends on the absorption coefficient by colored dissolved organic matter at 412 nm, and $\Delta_p(412)$ the residual terms accounting for the scattering and absorption of suspended marine particles on the $K_d(412)$ values. The effect of particulate scattering and absorption on $K_d(412)$ can be partially assessed using an appropriated wavelength, λ, at which colored dissolved organic matter has a negligible or limited effect due to the dominating impact of pure sea water and particulate IOPs. Among visible channels available on standard ocean color sensors, two wavelengths can be selected for that purpose: 555 nm and 670 nm. The ideal candidate would be the red channel, as colored dissolved organic matter does not absorb (or insignificantly) at 670 nm [16,44]. However, the signal-to-noise ratio at 670 nm is generally lower than that at 555 nm for current ocean color sensors [45,46]. Besides, the retrieval of the remote sensing reflectance is more challenging in the red than in the green, most likely due to the small level of signal in this part of the spectrum [47]. Formulations considering these two wavelengths will be tested and compared. In practice, for a peculiar wavelength, λ_p, we assume that:

$$K_d(\lambda_p) = K_w(\lambda_p) + \Delta_p(\lambda_p) \quad (3)$$

#208531 - $15.00 USD Received 18 Mar 2014; revised 9 May 2014; accepted 9 May 2014; published 22 May 2014

4.2 Development of the model from the synthetic data set DS1

The theoretical background and general formulation of the model presented in the previous section is now analyzed from radiative transfer simulations data gathered in DS1. While a_{cdom} will be estimated at 412 nm from the *in situ* database (section 4.2), the development based on DS1 is performed at 410 nm, the available wavelength in the blue. The pure sea water values of the vertical attenuation coefficient are set from radiative transfer simulations using the Hydrolight radiative transfer code [48] for a pure sea water body, different sun zenith angles, and in presence of Raman scattering. The resulting $K_w(\lambda)$ values at 410, 555, and 670 nm for a sun angle at 30° are 0.0097, 0.0645, and 0.4878 m^{-1}, respectively. These values are only slightly higher from those generally adopted in the literature ($K_w(410)$ = 0.00812 m^{-1}, $K_w(555)$ = 0.06053 m^{-1}, and $K_w(670)$ = 0.43946 m^{-1}) and calculated through the simple addition of pure sea water absorption and backscattering coefficients [38]. In Eq. (3) we assume that colored dissolved organic matter does not absorb (or insignificantly) at the considered wavelength, λ_p. Therefore, by simply removing $K_d(\lambda_p)$ to $K_d(410)$, part of the particulate impact on the variability of $K_d(410)$ should be removed (with however a strong wavelength dependence still remaining). From Eqs. (2) and (3) $a_{cdom}(410)$ can be expressed as follows:

$$a_{cdom}(410) = g\begin{bmatrix}(K_d(410) - K_w(410)) - (K_d(\lambda_p) - K_w(\lambda_p)) - \\ (\Delta_p(410) - \Delta_p(\lambda_p))\end{bmatrix} \quad (4)$$

A parameterization function of ($K_d(410)$-$K_w(410)$-($K_d(\lambda_p)$-$K_w(\lambda_p)$) has been developed in order to account for the impact of the particulate fraction ($\Delta_p(410)$-$\Delta_p(\lambda_p)$) on the $a_{cdom}(410)$ retrieval (Fig. 1).While other parameterizations were also tested to assess ($\Delta_p(410)$-$\Delta_p(\lambda_p)$), the latter ones has been found to be the more appropriated for remote sensing application (see discussion below). The sun angle dependence in the ($\Delta_p(410)$-$\Delta_p(\lambda_p)$) vs. f($K_d(410)$) relationship is relatively smaller for λ_p = 555 (Fig. 1c) than for λ_p = 670 nm (Fig. 1(a)).

#208531 - $15.00 USD Received 18 Mar 2014; revised 9 May 2014; accepted 9 May 2014; published 22 May 2014

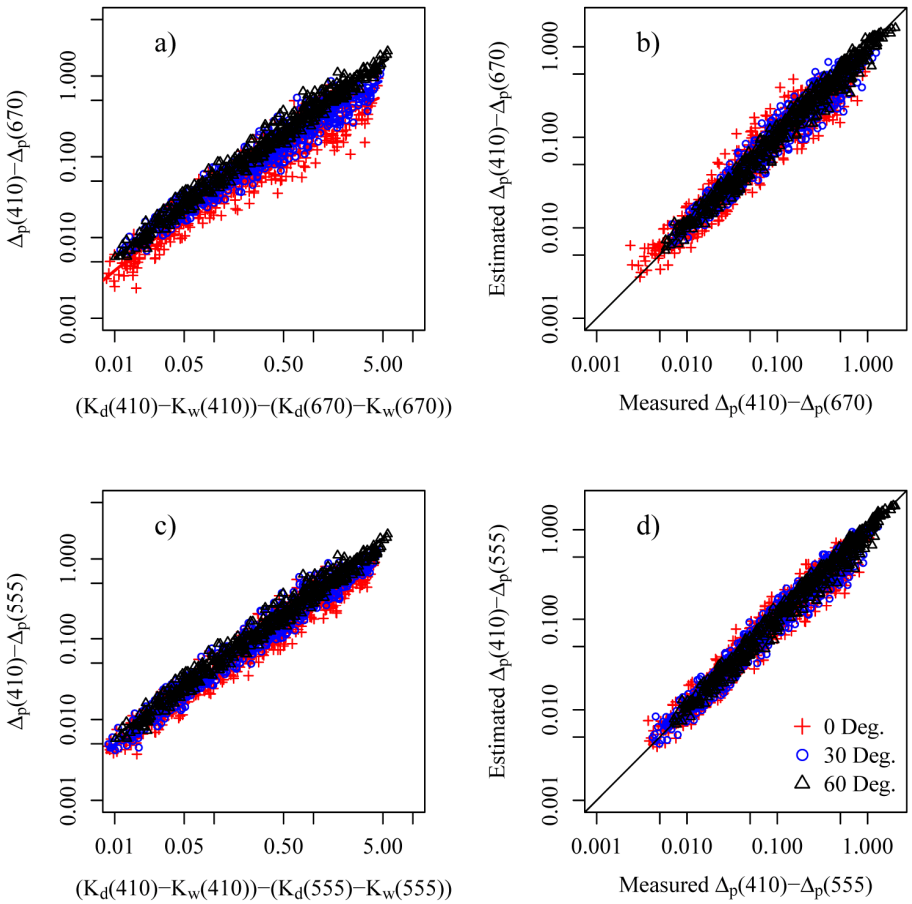

Fig. 1. (a) ($\Delta_p(410)$- $\Delta_p(670)$) as a function of ($K_d(410)$-$K_w(410)$-($K_d(\lambda_p)$-$K_w(\lambda_p)$) from the DS1 data set and for a sun zenith angle of 0°, 30°, and 60° as indicated. The solid lines are the best polynomial fits established for each sun angle. (b) scatter plot of ($\Delta_p(410)$- $\Delta_p(670)$), as retrieved using the polynomial function presented in Fig. 1(a), as a function of the true ($\Delta_p(410)$- $\Delta_p(670)$) values from the DS1 data set. The solid line represents the 1:1 line. The panels (c) and (d) are equivalent to panels (a) and (b), respectively, but for 555 nm.

The impact of each term of Eq. (4) on the accuracy of $a_{cdom}(410)$ retrieval is analytically examined from the synthetic data set DS1, which by nature is not affected by uncertainties measurements (Fig. 2). This cannot be considered as a validation exercise (as the same data set is used for the development and the evaluation), but rather to an evaluation of the actual impact of each step on the formulation proposed by Eq. (4). This will not be the case in the next section where the final algorithm will be develop and validated using two independents *in situ* data sets. The following statistical estimators are used for that purpose:

$$RMSD = \sqrt{\frac{\Sigma_{i=1}^{N}(y_i - x_i)^2}{N}}$$

$$MRAD = \frac{1}{N}\sum_{i=1}^{N}\frac{|y_i - x_i|}{x_i}\cdot 100$$

$$Bias = \frac{1}{N}\sum_{i=1}^{N}\frac{y_i - x_i}{x_i}\cdot 100$$

#208531 - $15.00 USD Received 18 Mar 2014; revised 9 May 2014; accepted 9 May 2014; published 22 May 2014

where x_i and y_i represents the measured and estimated parameters, respectively and N the total number of elements of the corresponding series.

The impact of the successive steps on the retrieval accuracy of $a_{cdom}(410)$ clearly appears in Fig. 2(a) and 2(c). Indeed, the whole data points get closer to the 1:1 line when the algorithm successively accounts for the different terms. The simple relationship between $a_{cdom}(410)$ and the first term of Eq. (4), $(K_d(410) - K_w(410))$, already allows $a_{cdom}(410)$ to be retrieved with a reasonable accuracy over the whole range of variability. The relative root mean square difference, RMSD, and Mean Relative Absolute Difference, MRAD, values for a sun angle at 30° are 0.12 m^{-1} and 23.47%, respectively. By accounting for the second term and third term of Eq. (4), $(K_d(\lambda_p) - K_w(\lambda_p))$ and $(\Delta_p(410)-\Delta_p(\lambda_p))$, the RMSD, and MRAD values are respectively 0.08 m^{-1} and 16.99%, using 670 nm (Fig. 2(b)), and 0.1 m^{-1} and 19.16%, using 555 nm (Fig. 2(d)).

The performance of the model does therefore not significantly change according to the choice of the examined λ_p wavelength. While $K_d(555)$ is still affected by absorption by colored dissolved organic matter ($a_{cdom}/a_{tot}(555) = 0.17 \pm 0.17$), the third term allows this residual effect to be taken into account. Among the three different terms appearing in the right side of Eq. (4), $(K_d(410) - K_w(410))$ represents the highest contribution to the whole term between bracket (thereafter referred as X). The median values calculated from the DS1 (at 30°) data set of $(K_d(410) - K_w(410))/X$, $(K_d(670) - K_w(670))/X$, and $(\Delta_p(410)-\Delta_p(670))/X$ are 1.78, 0.28, and 0.53, respectively. The median values calculated from the DS1 data set of $(K_d(555) - K_w(555))/X$, and $(\Delta_p(410)-\Delta_p(555))/X$ are 0.49, and 0.59, respectively. The final empirical equation used to assess $a_{cdom}(410)$ from K_d measurements performed at 410 and 555 nm, and a sun angle at 30° using the DS-1 data set is:

$$a_{cdom}(410) = 10^{\left[0.008 Log_{10}(X)^2 + 1.017 Log_{10}(X) + 0.0416\right]} \quad (5)$$

where $X = (K_d(410) - K_w(410)) - (K_d(555) - K_w(555)) - (\Delta_p(410)-\Delta_p(555))$

#208531 - $15.00 USD Received 18 Mar 2014; revised 9 May 2014; accepted 9 May 2014; published 22 May 2014

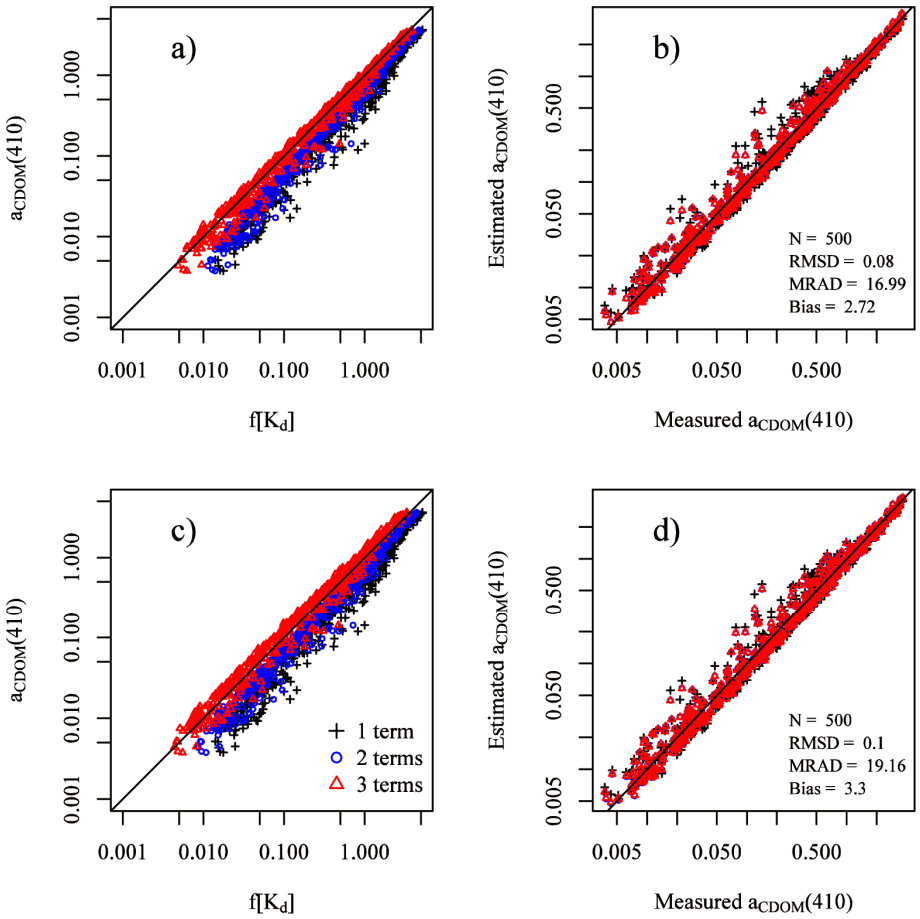

Fig. 2. (left panel) (a) Scatter plots of $a_{cdom}(410)$ as a function of$(K_d(410) – K_w(410))$ in black, $(K_d(410) - K_w(410)) – ((K_d(670)-K_w(670))$ in blue, and $(K_d(410) - K_w(410)) - (K_d(670) - K_w(670)) - (\Delta_p(410)-\Delta_p(670))$ in red, for the DS1 data set and a sun zenith angle at 30°. (c) as in (a) but where the 555 wavelength is used instead of 670. (right panels) scatter plot of the estimated values of $a_{cdom}(410)$ calculated at each successive step describe in the left panels as a function of the true $a_{cdom}(410)$ values. The solid line represents the 1:1 line. The statistical indicators are provided as indicated for a sun angle at 30°.

4.3 Development of the model from the in situ data set

The evaluation of the impact of each term of Eq. (4) is now performed using the *in situ* data set DS2-D. Considering that the performance of the method established from DS1 is relatively similar for red and green channels and the greater complexity to assess K_d from space in the red part of the spectrum, this part will only focus on the green channel. The advantage of each step on the proposed approach is summarized in Fig. 3. As for the synthetic data set, a tight relationship is observed between $a_{cdom}(410)$ and $(K_d(410) - K_w(410))$ over the whole range of variability of DS2-D (Fig. 3(a)). Note that this relationship slightly differs from the one established using the synthetic data set. The inherent uncertainties associated with *in situ* measurements, but also the relationship between a_{cdom} and absorption by phytoplankton cells used in the synthetic data set [24], are at the origin of the observed discrepancies.

#208531 - $15.00 USD Received 18 Mar 2014; revised 9 May 2014; accepted 9 May 2014; published 22 May 2014

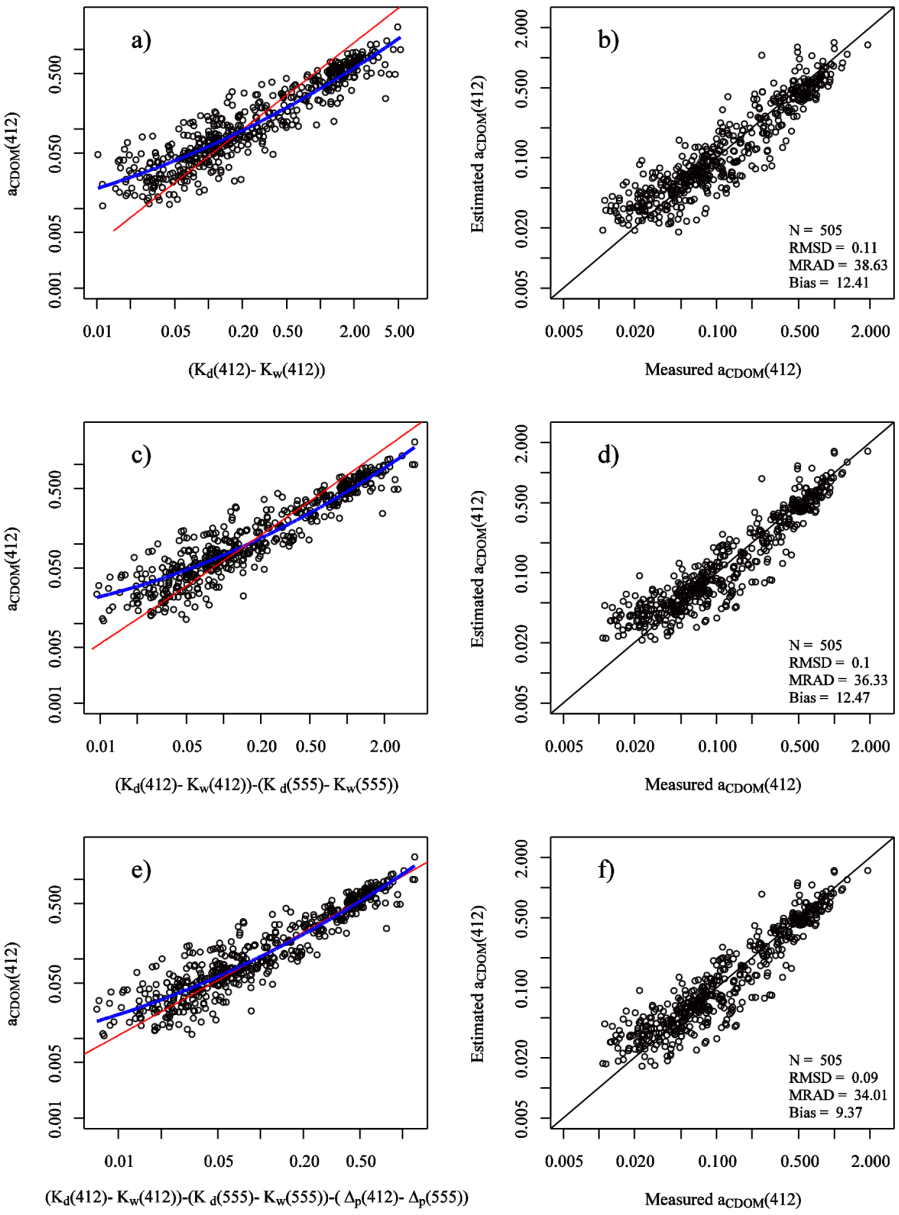

Fig. 3. (left panel) Scatter plots of $a_{cdom}(412)$ as a function of (a) ($K_d(412) - K_w(412)$), (c) ($K_d(412)$ - $K_w(412)$) - ($K_d(555)$ - $K_w(555)$) and (e) ($K_d(412)$ - $K_w(412)$) - ($K_d(555)$ - $K_w(555)$) - ($\Delta_p(412)$-$\Delta_p(555)$) for the DS2-D in situ data set (right panels) Scatter plot of the estimated values of $a_{cdom}(412)$ calculated from the (b) first, (d) second, and (f) last step of the algorithm. The red lines in the left panels represent the fitted curves obtained from the DS1 data set, and the blue lines represent the best fits on the DS2-D data set.

The RMSD, MRAD, and bias decrease from the first step to the last one by a factor of 1.22 (RMSD = 0.09 m^{-1}), 1.13 (MRAD = 34.01%), and 1.32 (bias = 9%). To quantitatively assess the impact of turbidity on the performance of the model, the whole data set is split into four equal parts computed according to Hyndman and Fan recommendation [49]. The RMSD, MRAD, and bias values for the sub-data sets characterized by the highest (and lowest) $a_p(410)/a_{cdom}(410)$ values are 0.1(0.06) m^{-1}, 40(37)% and 36 (–24)%. These values globally agree with the ones calculated for the whole data set. The small impact (at least on the present

#208531 - $15.00 USD Received 18 Mar 2014; revised 9 May 2014; accepted 9 May 2014; published 22 May 2014

data sets) of turbidity on the $a_{cdom}(410)$ vs. ($K_d(412)$ - $K_w(412)$) relationship is explained by the fact that turbid waters in coastal areas are generally associated with a high concentration of *CDOM* (and vice versa) [16]. The bias values for the first and last quartile significantly differ from the one established from the whole data set. This latter pattern emphasizes that a residual effect of the particulate matter still remains. Such effect, inherent to all empirical approaches [11], could however be corrected through classification approaches [28,50].

Based on these different findings the following relationship, developed from the *in situ* data set DS2-D, is adopted:

$$a_{cdom}(412) = 10^{\left[0.1548 Log_{10}(X)^2 + 1.1939 Log_{10}(X) + 0.0689\right]} \quad (6)$$

with $X = (K_d(412) - K_w(412)) - (K_d(555) - K_w(555)) - (\Delta_p(412) - \Delta_p(555))$

and with $(\Delta_p(412) - \Delta_p(555))$ estimated such as:

$$\Delta_p(412) - \Delta_p(555) = 10^{\left[-0.009 Log_{10}(Y)^2 + 1.147 Log_{10}(Y) - 0.26\right]} \quad (7)$$

where $Y = (K_d(412) - K_w(412) - (K_d(555) - K_w(555))$. The slight differences observed in the coefficients appearing in Eqs. (5) and 6 are mainly explained by the assumptions used to generate a_{cdom} from a_{phy} in the synthetic data set (DS1), which may not be totally adapted to cover the whole type of waters in DS2 [24].

5. Validation and comparison with previous algorithms

5.1 Using K_d as input parameters

The model presented in Eq. (6) is now tested against an independent data set, DS2-V, previously presented in Table 1. The RMSD, MRAD, and bias values are 0.09 m^{-1}, 33.6%, and 17.7%, respectively for the final $a_{cdom}(412)$ estimated values. Consistently with the synthetic data set, the performance of the $a_{cdom}(412)$ retrieval is improved with the successive steps of the algorithms (Fig. 4). The use of the parameterization considering $K_d(555)$-$K_w(555)$ and $(\Delta_p(412) - \Delta_p(555))$ rather than the expression only based on $K_d(412)$ decreases the RMSD, MRAD and bias by a factor 1.33, 1.21, and 1.37, respectively.

#208531 - $15.00 USD Received 18 Mar 2014; revised 9 May 2014; accepted 9 May 2014; published 22 May 2014

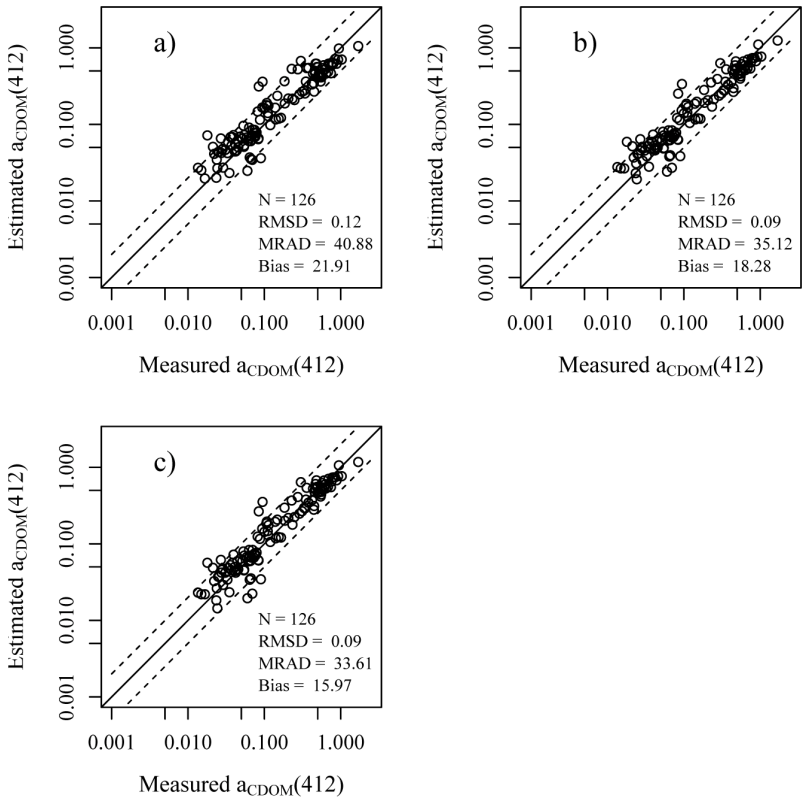

Fig. 4. Scatter plots of $a_{cdom}(412)$ estimated at the (a) first, (b) second and (c) last step of the model, as a function of *in situ* measurements. The solid line represents the 1:1 line. The dashed lines represent the 1:2 and 2:1 lines.

5.2 Using R_{rs} as input parameters

The model is now tested in the context of ocean color remote sensing observations, where K_d is not directly measured, but instead estimated from R_{rs}. Different approaches presented in section 3 have been developed to assess K_d at different wavelengths from ocean color observations. Because of the structure of the present model (Eq. (6), the errors on the estimation of K_d at each wavelength are additive. To limit this impact, the K_d differences appearing in Eq. (6) are directly assessed from R_{rs} using a new parameterization developed from the IOCCG (2006) data set:

$$\left((K_d(412)-K_w(412))-(K_d(555)-K_w(555))\right)= 10^{\left[A.Log_{10}\left(\frac{R_{rs}(412)}{R_{rs}(555)}\right)^3+B.Log_{10}\left(\frac{R_{rs}(412)}{R_{rs}(555)}\right)^2+C.Log_{10}\left(\frac{R_{rs}(412)}{R_{rs}(555)}\right)+D\right]} \quad (8)$$

The (A, B, C, D) coefficients values are (–0.0634808, 0.254858, –1.22384, –0.89454), (–0.12484, 0.160857, –1.2292, –0.886471), and (–0.535652, –0.224119, –1.18114, –0.840784) for sun zenith angles, θ_0, of 0°, 30°, and 60°, respectively. In the frame of remote sensing applications, the coefficients values calculated for θ_0 = 0° should be taken, as the provided R_{rs} values are generally normalized for a sun at zenith. The performances of the new algorithm in the context of ocean color remote sensing observations are summarized in Table 2 and Fig. 5. Comparison with two empirical [4,17] and one semi-analytical existing algorithms [22] is also provided.

#208531 - $15.00 USD Received 18 Mar 2014; revised 9 May 2014; accepted 9 May 2014; published 22 May 2014

Table 2. Statistics computed on the D2-V data set using the algorithm defined in this study and those documented previously, values in brackets indicate the statistics computed from these models adjusted to our data set.

	This Study	Mannino et al. (2008)	D'Sa et al. (2006)	Dong et al. (2013)
RMSD (m^{-1})	0.21	0.19 (0.12)	0.19 (0.18)	0.24
MRAD (%)	42.82	90.6 (69.18)	87.7 (59.85)	51.6
Bias (%)	7.12	12.46 (31. 19)	73.03 (33.4)	0.42
N	126	121 (100)	126	126

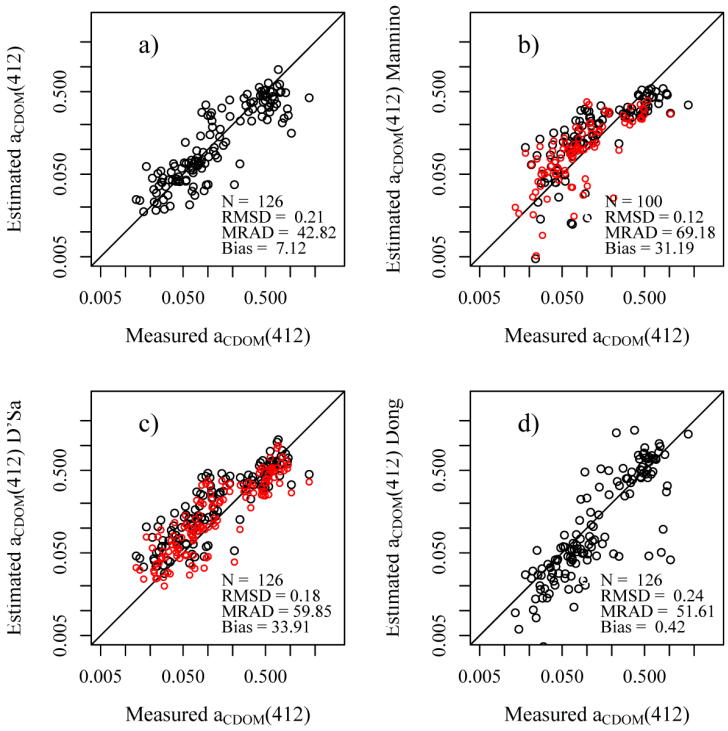

Fig. 5. Comparison of the modeled and the measured $a_{cdom}(412)$ from the D2-V data set using (a) the present algorithm, (b) the Mannino et al. [4]'s algorithm, (c) the D'Sa et al. [17]'s algorithm, and (d) the Dong et al. [22]'s algorithm. For the two empirical algorithms [4,17], the black dots are for the original algorithm and the blue ones when their coefficients are adapted to the DS2-D data set used for the algorithm development.

While the a_{cdom} retrieval values are slightly better when K_d is measured (Fig. 4(c)) than when it is inversed (Fig. 5(a)), they are still in good agreement with field measurements. All the data points are well distributed along the 1:1 line. The RMSD, MRAD, and bias values are 0.21 m^{-1}, 42.82%, and 7.12%, respectively considering the whole model description. The two previously published algorithms developed for the U.S. Middle Atlantic Bight waters [4], and

Table 3. Statistics computed on the NOMAD Matchup (N = 109) data set using the algorithm defined in this study and those documented previously and adjusted to our development data set (see Fig. 6).

	This Study[a]	This Study[b]	Mannino et al. (2008)	D'Sa et al.(2006)	Dong et al. (2013)
RMSD (m^{-1})	0.13	0.11	0.08	0.11	0.17
MRAD (%)	48.26	37.1	47.93	63.49	54.33
Bias (%)	28.77	10.55	17.9	48.69	21.5
N	109	109	101	109	108

[a]Using $R_{rs}(412)/R_{rs}(555)$ in Eq. (8). [b]Using $R_{rs}(443)/R_{rs}(555)$ in Eq. (8)

#208531 - $15.00 USD Received 18 Mar 2014; revised 9 May 2014; accepted 9 May 2014; published 22 May 2014

coastal waters under the influence of the Mississippi river [17], that is for two specific coastal areas, performed also relatively well, in spite of relatively higher MRAD and bias values (Fig. 5 (b), (c), and Table 2). However, by fitting the empirical formulations used in these a_{cdom} vs. R_{rs} empirical models to the DS2-D data set, their performances evaluated on DS2-V improve. For instance, the RMSD values decrease by a factor of 1.58, and 1.06 for the models of Mannino et al. [4], and D'Sa et al. [17], respectively. The formulation between R_{rs} and a_{cdom} used in these models are therefore relatively dependent on the data set used for their development. Note that the number of validation data points is reduced for Mannino et al., [4]'s algorithm which, by construction, cannot be applied when the $R_{rs}(490)/R_{rs}(555)$ ratio becomes lower than 0.4443 (resulting to a logarithmic calculation of a negative expression). The recent semi-analytical approach developed by Dong et al. [22], also shows relatively good performance over the present data set, with a Mean Relative Absolute Difference of 51% (against 70 and 60% for the approaches of Mannino et al. [4], and D'Sa et al. [17], respectively, when their coefficients are adapted to the present data set).

Similar results are also obtained using the NOMAD matchup data set which includes uncertainties related to atmospheric corrections (Fig. 6, Table 3). Note that the use of a reflectance ratio in Eq. (8) reduces the impact of R_{rs} uncertainties on the a_{cdom} retrieval accuracy. Due to the fact that $R_{rs}(412)$ is generally more affected by atmospheric correction errors than $R_{rs}(443)$ [47], the $R_{rs}(443)/R_{rs}(555)$ ratio can also be used instead of $R_{rs}(412)/R_{rs}(555)$ in Eq. (8). In this case, the (A, B, C, D) coefficients values are (−0.2925, 0.4015, −1.365, −0.863) for a sun at zenith. However, while $a_{cdom}(412)$ retrieval is improved (see Table 3), the dynamics toward high $a_{cdom}(412)$ values is reduced. Considering the present approach, the tight link between K_d and a_{cdom} is theoretically expected, and confirmed from synthetic and *in situ* data sets. The accuracy of our model is tightly linked to the retrieval accuracy of K_d, and depends on the quality of the empirical relationships adopted (Eqs. (6) and (7)). The dispersion observed around these relationships is mainly explained by the residual impact of the absorption and scattering properties of particulate matter, even though this effect is greatly reduced from step 1 to step 3 (see Fig. 2).

As atmospheric correction is one of the main challenges for the exploitation of ocean color remote sensing over coastal areas, the impact of potential atmospheric correction errors on the $a_{cdom}(412)$ retrieval should be assessed. According to the ESA (2012) [51] validation report, the relative percentage differences calculated between the estimated and measured reflectance values in coastal waters at 412 and 560 nm are + 1.6% and −6.3%, respectively. The impact of these errors on the $a_{cdom}(412)$ retrieval accuracy is assessed using the validation data set DS2-V, by comparing the $a_{cdom}(412)$ values calculated using the true R_{rs} values, $a_{cdom}(412)$-error-free, with the $a_{cdom}(412)$ values calculated using these R_{rs} values modified by the relative differences provided above, $a_{cdom}(412)$-error. These atmospheric correction errors only slightly impact the $a_{cdom}(412)$ retrieval accuracy, as the mean relative absolute difference and bias values calculated between these two $a_{cdom}(412)$ values in linear scale are 8.68% and 8.68%, respectively. The median value of the ($a_{cdom}(412)$-error- $a_{cdom}(412)$free)/$a_{cdom}(412)$-error is −8.67% ± 2.95% on the validation data set.

#208531 - $15.00 USD Received 18 Mar 2014; revised 9 May 2014; accepted 9 May 2014; published 22 May 2014

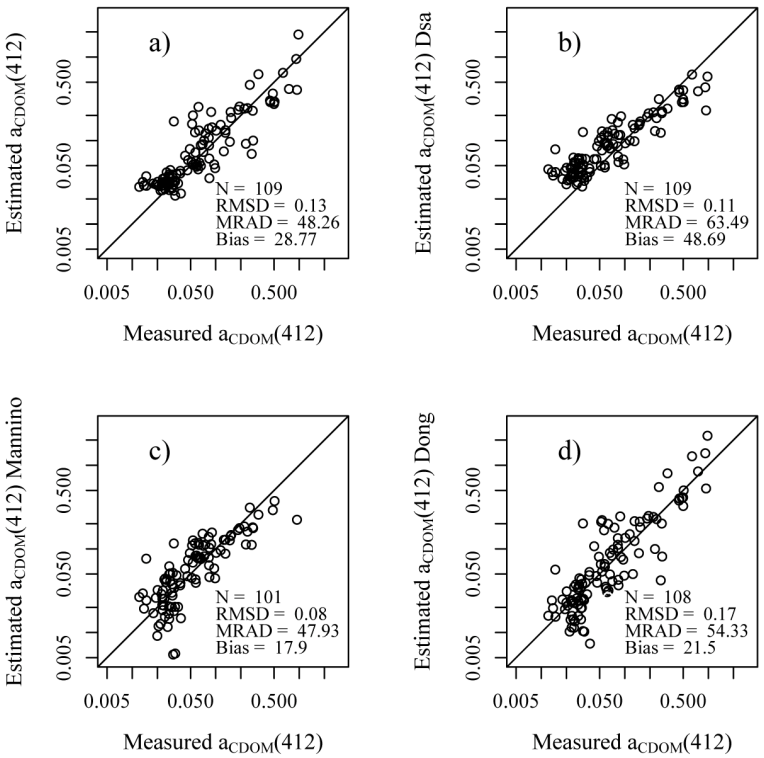

Fig. 6. As for Fig. 5 but using the NOMAD-Matchup data set. The parameters used in the empirical algorithms presented in panels b) and c) have been adapted to the present data set (see text).

6. Concluding remarks

A new model has been developed to assess the colored dissolved organic matter in natural waters from the vertical attenuation coefficient of the downwelling irradiance, K_d. A theoretical background has been defined to relate a_{cdom} to a combination of K_d at 412 and 555 nm. The development of the a_{cdom} vs. K_d relationships is based on a large in situ data set (N = 505) gathering measurements performed in various costal environments. In the frame of ocean color remote sensing applications, only R_{rs} is available, and then K_d has first to be estimated. This model can only be applied for the range of $a_{cdom}(412)$ considered here, that is about [0.02; 5.0 m^{-1}]. The performance of this model has been successfully tested using a relatively large in situ data set (N = 126) and the Nomad match-up data set (N = 109) covering very contrasted coastal environments.

Acknowledgments

The authors would like to thank all participants and voluntary contributors for collecting data that have been assembled in the NOMAD data set. This study has been performed in the frame of the GlobCoast (www.foresea.fr/globcoast) which is funded by the Agence Nationale de la Recherche (ANR-11-BLAN-BS56-018-01). The GlobCoast project is affiliated to LOICZ and AQUIMER. This work has also been supported by the French Spatial Agency (CNES) through the TOSCA program in the frame of the MODOC project. S. Shang is deeply thanked for providing us the results of the Dong et al. (2013)'s model. We thank the two anonymous reviewers for their comments and suggestions.